AFRL-RX-WP-TP-2010-4160

TRAPPING AND ESCAPE OF DISLOCATIONS IN MICRO-CRYSTALS WITH EXTERNAL AND INTERNAL BARRIERS (PREPRINT)

Christopher Woodward, Dennis M. Dimiduk, and Michael D. Uchic

Metals Branch
Metals, Ceramics & NDE Division

Jaafar A. El-Awadya

Universal Technology Corporation

Satish I. Rao

UES

FEBRUARY 2010

AIR FORCE RESEARCH LABORATORY
MATERIALS AND MANUFACTURING DIRECTORATE
WRIGHT-PATTERSON AIR FORCE BASE, OH 45433-7750
AIR FORCE MATERIEL COMMAND
UNITED STATES AIR FORCE

REPORT DOCUMENTATION PAGE

Form Approved
OMB No. 0704-0188

1. REPORT DATE *(DD-MM-YY)*	2. REPORT TYPE	3. DATES COVERED *(From - To)*
February 2010	Journal Article Preprint	01 February 2010 – 28 February 2010

4. TITLE AND SUBTITLE
TRAPPING AND ESCAPE OF DISLOCATIONS IN MICRO-CRYSTALS WITH EXTERNAL AND INTERNAL BARRIERS (PREPRINT)

5a. CONTRACT NUMBER
In-house

5b. GRANT NUMBER

5c. PROGRAM ELEMENT NUMBER
62102F

6. AUTHOR(S)
Christopher Woodward, Dennis M. Dimiduk, and Michael D. Uchic (AFRL/RXLM)
Jaafar A. El-Awadya (Universal Technology Corporation)
Satish I. Rao (UES)

5d. PROJECT NUMBER
4347

5e. TASK NUMBER
RG

5f. WORK UNIT NUMBER
M02R1000

7. PERFORMING ORGANIZATION NAME(S) AND ADDRESS(ES)
Metals Branch (AFRL/RXLM)
Metals, Ceramics & NDE Division
Materials and Manufacturing Directorate
Wright-Patterson Air Force Base, OH 45433-7750
Air Force Materiel Command, United States Air Force

Universal Technology Corporation
1270 North Fairfield Road
Dayton, OH 45432-2600

UES
4401 Dayton-Xenia Road
Dayton, OH 45432-1894

8. PERFORMING ORGANIZATION REPORT NUMBER
AFRL-RX-WP-TP-2010-4160

9. SPONSORING/MONITORING AGENCY NAME(S) AND ADDRESS(ES)
Air Force Research Laboratory
Materials and Manufacturing Directorate
Wright-Patterson Air Force Base, OH 45433-7750
Air Force Materiel Command
United States Air Force

10. SPONSORING/MONITORING AGENCY ACRONYM(S)
AFRL/RXLMD

11. SPONSORING/MONITORING AGENCY REPORT NUMBER(S)
AFRL-RX-WP-TP-2010-4160

12. DISTRIBUTION/AVAILABILITY STATEMENT
Approved for public release; distribution unlimited.

13. SUPPLEMENTARY NOTES
Journal article submitted to *International Journal of Plasticity*. PAO Case Number: 88ABW-2010-0351; Clearance Date: 27 Jan 2010. Paper contains color.

14. ABSTRACT
We perform three-dimensional dislocation dynamics simulations of solid and annular pillars, having both free surface boundary conditions, or strong barriers at the outer and/or inner surfaces. Both pillar geometries are observed to exhibit a size effect where smaller pillars are stronger. The scaling observed is consistent with the weakest-link activation mechanism and depends on the solid pillar diameter, or the annular pillar effective diameter, Deff= D–Di. An external strong interface is observed to dramatically increase the dislocation density by an order of magnitude due to trapping dislocations at the interface. In addition, a considerable increase in the flow strength by up to 60% from simulations having free surface boundary conditions is observed. As the applied load increases, weak spots form on the surface of the pillar by dislocations breaking through the interface when the RSS is greater than the barrier strength. The hardening rate is also observed to increase with increasing interface strength.

15. SUBJECT TERMS
dislocation dynamics, micropillar coating, size effects, plasticity

16. SECURITY CLASSIFICATION OF:			17. LIMITATION OF ABSTRACT:	18. NUMBER OF PAGES	19a. NAME OF RESPONSIBLE PERSON (Monitor)
a. REPORT	b. ABSTRACT	c. THIS PAGE			Christopher F. Woodward
Unclassified	Unclassified	Unclassified	SAR	48	19b. TELEPHONE NUMBER *(Include Area Code)* N/A

Standard Form 298 (Rev. 8-98)
Prescribed by ANSI Std. Z39-18

Trapping and escape of dislocations in micro-crystals with external and internal barriers

Jaafar A. El-Awady[a,b], Satish I. Rao[a,c], Christopher Woodward[a], Dennis M. Dimiduk[a], Michael D. Uchic[a]

[a] *Air Force Research Laboratory, Materials and Manufacturing Directorate, AFRL/RXLM Wright-Patterson AFB, OH 45433-7817, USA*
[b] *Universal Technology Corporation, 1270 North Fairfield Road, Dayton, OH 45432-2600*
[c] *UES, 4401 Dayton-Xenia Rd, Dayton, OH 45432-1894*

Abstract

We perform three-dimensional dislocation dynamics simulations of solid and annular pillars, having both free surface boundary conditions, or strong barriers at the outer and/or inner surfaces. Both pillar geometries are observed to exhibit a size effect where smaller pillars are stronger. The scaling observed is consistent with the weakest-link activation mechanism and depends on the solid pillar diameter, or the annular pillar effective diameter, $D_{eff} = D - D_i$, where D and D_i are the external and internal diameters of the pillar, respectively. An external strong barrier is observed to dramatically increase the dislocation density by an order of magnitude due to trapping dislocations at the surface. In addition, a considerable increase in the flow strength by up to 60% from simulations having free surface boundary conditions is observed. As the applied load increases, weak spots form on the surface of the pillar by dislocations breaking through the surface when the RSS is greater than the barrier strength. The hardening rate is also observed to increase with

Email address: Jaafar.El-Awady@wpafb.af.mil (Jaafar A. El-Awady)

increasing barrier strength. With cross-slip, we observe dislocations moving to other glide planes, and sometimes double-cross slipping, producing a thickening of the slip traces at the surface. Finally the results are in qualitative agreement with recent compression experimental results of coated and centrally filled micropillars.
Key words: Dislocation Dynamics, Micropillar Coating, Size Effects, Plasticity

---

1. Introduction

Recently, Uchic et al. (2004) developed a new experimental methodology, to study the flow behavior of micron-sized crystals. In this methodology, micron scale samples were fabricated with a Focused Ion Beam (FIB), then tested under uniaxial compression using a nano-indentation system equipped with a flat ended diamond tip (Uchic et al., 2003, 2004; Uchic and Dimiduk, 2005). This methodology sparked a wide interest in the plasticity and size effects at micron-scales, from both the experimental and modeling perspectives. A myriad of adaptations to this methodology have been applied to study a variety of materials, and to address different aspects of the plasticity at such small scales (Uchic et al., 2009; Oh et al., 2009; Shim et al., 2009; Ng and Ngan, 2009; Shade et al., 2009).

From these experimental results, a consistent size-dependency of the flow strength on the sample diameter was observed (Uchic et al., 2009). In addition, the flow strength was observed to be stochastic in nature, with the micro samples deforming through discontinuous events that span several orders of magnitude in size. To explain such unusual observations, Greer et al.

(2005) proposed the idea of dislocation starvation. In this hypothesis it was assumed that dislocations escape the pillars faster than they can multiply, thus, leaving the pillars dislocation free, and much stronger. Although, for pillars having diameters smaller than $D = 0.2$ μm, some experimental observations seem to agree with this hypothesis (Shan et al., 2008; Lee et al., 2009), it was later set aside in the case of larger pillars (Uchic et al., 2009). From both theoretical studies and dislocation dynamics simulations (Benzerga and Shaver, 2006; Parthasarathy et al., 2007; El-Awady et al., 2008; Rao et al., 2008; Tang et al., 2008; El-Awady et al., 2009; Uchic et al., 2009; Benzerga, 2009) it was argued that the strengthening and stochastic effects observed in experiments, can be explained by the activation and subsequent exhaustion of dislocations from the weakest sources available in the crystal. These sources are typically double-pinned FrankRead sources, or truncated single dislocation arms that are pinned from one end inside the crystal and terminating at the surface from the other end. This has been referred to as the "weakest-links activation mechanism". This was also confirmed by transmission electron microscopy (TEM) observations of compressed pillars (Norfleet et al., 2008). In addition, recent *in situ* tension experiments of sub-micron Al crystals (Oh et al., 2009) validated the stochastic effect and the source truncation mechanism identified through dislocation dynamic simulations.

The current authors have recently performed detailed analysis to study the effects of different initial dislocation densities and dislocation-source lengths on the size scaling and stochastic response of micropillars (Parthasarathy et al., 2007; Rao et al., 2008; El-Awady et al., 2009). In addition to linking the flow strength size-scaling to the weakest-dislocation-links available in the

micropillar, it was also shown that for a higher initial dislocation density a low scaling response is observed, and vice versa. For large pillar sizes, simulations having high initial dislocation densities were observed to result in a high flow stress. This is due to the dominance of forest-hardening processes for these larger pillars. Such trend is reversed at smaller sizes were higher dislocation densities will result in a weaker pillar. They also observed that the scatter is considerably less for high dislocation density simulations compared with low-density simulations. Such a barrier may be unintentionally formed as in the case of an amorphous layer which is a byproduct of milling using a Focused Ion Beam (FIB) on some materials (Rubanov and Muroe, 2004; Maaβ et al., 2006; Kiener et al., 2007), or intentionally formed by coating/filling the specimen with a material that is much stronger than its bulk (Baker et al., 2003; Nicola et al., 2006; Ng and Ngan, 2009). In particular, attention will be given to the influence of such barriers on the flow strength and work-hardening.

Previously, Nicola et al. (2003, 2006) performed two-dimensional dislocation dynamics simulations to study the effect of impenetrable boundaries on the plastic deformation in freestanding thin films. Although, such observations provide some insight on the effect of the presence of strong interfaces, they do not account for important three-dimensional effects (Nix, 1998). These include the complex character of the dislocations, line tension, and the interaction of dislocations not parallel to existing misfit dislocation lines along the interface. In addition, Espinosa et al. (2006) performed three-dimensional dislocation dynamics simulations to study the size effects in freestanding films. These simulations were carried out on rectangular sim-

ulation cells corresponding to a columnar grain, and the grain boundaries were assumed impenetrable. The initial conditions of these simulations included placing all dislocation sources at the grain boundaries with the bulk left initially free from any dislocation sources. Such assumptions are not consistent with experimental observed dislocation structures and densities found in bulk crystals and micropillars (Dimiduk et al., 2005; Greer et al., 2005; Norfleet et al., 2008; Oh et al., 2009), or the fact that dislocations can escape by being transmitted across the boundary (de Koning et al., 2002).

In the following, we will study these effects by performing three-dimensional (3D) dislocation dynamics (DD) simulations of solid and annular pillars. The influence of the strength of the pillar surface on dislocation evolution, work-hardening and stress will be examined parametrically. In addition, the effect of cross-slip activation is also discussed. In Section 2, we first give a brief outline of the computational method and the setup of the computer simulations. Then, in Section 3, the simulation results, including the stress-strain behavior, dislocation density versus strain relationship, and dislocation microstructure evolution are discussed in detail. Finally, a discussion and conclusions are given in Section 4.

2. Computational Method and Problem Setup

In order to properly treat the dislocation free surfaces, the Boundary Element Method (BEM) is coupled with a three-dimensional (3D) Parametric Dislocation Dynamics (PDD) method. This methodology, recently developed by El-Awady et al. (2008), is well suited for studies of plastic deformation in small volumes. In this technique, the total stress and displacement fields

are evaluated as the superposition of the elastic field in an infinite medium generated by all dislocation loops in the finite volume, and the correction field resulting from enforcing the boundary conditions. The elastic field of a dislocation loop is computed using the fast-summation method developed by Ghoniem and Sun (1999). The correction field is then obtained by inverting the traction on the surface of the finite volume produced by all dislocation loops in the system and solving a system of boundary integral equations within the framework of the BEM to account for the correct displacement and traction boundary conditions. Finally, the total stress and hence total force on each dislocation loop can be computed (El-Awady et al., 2008). Subsequently, the evolution of the microstructure can then be obtained using the framework of the PDD method by solving a quasi-static equation of motion that relates the velocity of the dislocation to the forces acting on it through a viscous drag relationship. In FCC crystals, the dislocation mobility (inverse of resistivity) can be assumed to be spatially isotropic, and the dislocation resistivity is on the order of 510^{-5} Pa s. Further details on the computational method can be found elsewhere (Ghoniem and Sun, 1999; Ghoniem et al., 2000; El-Awady et al., 2008).

All the following simulations are carried out in solid and annular cylindrical micropillars. These micropillars are assumed to be face-centered-cubic (FCC) single-crystals, oriented for multi-slip with the [001] direction parallel to the micropillar axis. The crystal properties used in the simulations are those of nickel. A schematic of the geometries of the simulated micropillars are shown in Figure 1. The aspect ratio in all simulations is fixed at $L : D = 3 : 1$. For the solid cylindrical geometry, the pillar diameter is var-

ied from $D = 0.25$ to 5.0 μm. On the other hand, the annular pillars external diameter is fixed at $D = 1.0$ μm, while the internal diameter is varied such that $D_i = 0.1$, 0.25, and 0.5 μm, respectively.

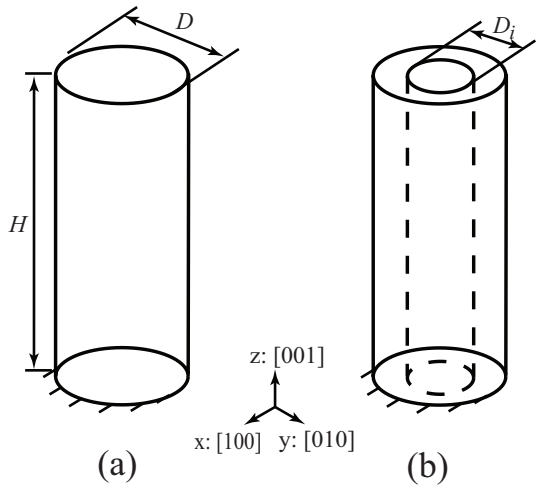

Figure 1: Schematic of the simulated single-crystal micropillars oriented in the [001] directions: (a) solid micropillar; and (b) annular micropillar. A constant aspect ration of $L : D = 3 : 1$ in all simulations.

The initial dislocation microstructure was generated by randomly populating all slip systems with single-ended and double-ended sources, having a random length, λ, such that $0 \leqq \lambda/D \leqq 0.5$ (El-Awady et al., 2009). Three initial dislocation densities were used for simulations of solid micropillars having sizes between $D = 0.25$, and 1.0 μm as summarized in 1. Due to the intense and time consuming computations required for the larger, $D = 5.0$ μm solid micropillar, only one initial dislocation density of 1.6 $\times 10^{12}$ m^{-2} was used for these simulations. For reference purposes later on in this paper, simulations with the lower dislocation density in each micropillar will be

termed "Case 1", and simulations with the intermediate dislocation density will be termed "Case 2", while those with higher densities will be termed "Case 3" as noted in 1.

Table 1: Initial dislocation density of the simulated solid micropillars

D μm	Case 1	Case 2	Case 3
0.25	6.7 $\times 10^{12}$ m^{-2}	9.7 $\times 10^{12}$ m^{-2}	11.5 $\times 10^{12}$ m^{-2}
0.5	3.8 $\times 10^{12}$ m^{-2}	6.7 $\times 10^{12}$ m^{-2}	11.5 $\times 10^{12}$ m^{-2}
0.75	1.3 $\times 10^{12}$ m^{-2}	6.7 $\times 10^{12}$ m^{-2}	11.5 $\times 10^{12}$ m^{-2}
1.0	1.0 $\times 10^{12}$ m^{-2}	1.1 $\times 10^{12}$ m^{-2}	3.7 $\times 10^{12}$ m^{-2}

The initial dislocation microstructure of the annular micropillars were generated from the $D = 1.0$ μm solid micropillars by carving out a cylindrical volume with the desired internal diameter along the center. One annular micropillar having $D_i = 0.5$ μm, was generated from the $D = 1.0$ μm solid micropillar having initial density of 1.0×10^{12} m^{-2}. The resulting initial dislocation density was 1.3×10^{12} m^{-2}. On the other hand, three annular micropillars having $D_i = 0.1$, 0.25, and 0.5 μm, were carved out of the $D = 1.0$ μm solid micropillar having initial density of 3.7×10^{12} m^{-2}. The resulting initial dislocation density for the annular pillars were 3.74, 3.95, and 3.83 $\times 10^{12}$ m^{-2}, respectively.

A compressive stress is applied in the [001] direction, while the bottom of the simulated pillar are assumed fixed. Consistent with previous micro-compression experiments and simulations, the compressive stress is applied through a mixture of a strain controlled- and a stress controlled-type of loading (Uchic et al., 2004; Uchic and Dimiduk, 2005; Rao et al., 2008). First,

a constant strain rate, $\dot{\varepsilon}$, is imposed and the rate of loading is computed from

$$\dot{\sigma} = E(\dot{\varepsilon} - \dot{\varepsilon}_p) \tag{1}$$

where $\dot{\sigma}$ is the applied stress rate, E is the elastic modulus of the material, and $\dot{\varepsilon}_p$ is the plastic strain rate which is proportional to the total area swept by the dislocations in the system. At any subsequent time step, if the calculated plastic strain rate is smaller than the applied strain rate, (i.e. $\dot{\varepsilon}_p < \dot{\varepsilon}$), the rate of loading is computed again following equation (1). On the other hand, if this computed plastic strain rate is greater than the applied strain rate, (i.e. $\dot{\varepsilon}_p > \dot{\varepsilon}$), the rate of loading is set to zero. This condition is then maintained until the computed total strain becomes equal to or greater than the applied strain rate multiplied by the elapsed time, (i.e. $(\varepsilon_e + \varepsilon_p) < \dot{\varepsilon}\Delta t$). This loading sequence is then repeated throughout the simulation. The constant strain rate used in the current simulations was set at $\dot{\varepsilon} = 50\ s^{-1}$.

3. Simulation Results

In our simulations, the strong barrier is assumed to be impenetrable by dislocations moving in the bulk of the pillar, as long as the resolved shear stress (RSS) is below a critical value, σ_c. This stress is the Koehler barrier strength required for a dislocation to break through the interface between the pillar and the stronger outer layer. Such strengthening effect is attributed to the elastic modulus mismatch across the interface, lattice resistance mismatch influencing the core structure, and any coherency strains (Rao and Hazzledine, 2000). From atomistic simulations of Cu-Ni multilayered systems (Rao and Hazzledine, 2000), it was reported that this barrier strength, σ_c,

can range between 15 to 60 times higher than the bulk strength, σ_b, depending on the thickness of the layers, dislocation character, and the interface orientation. This is also consistent with dislocation dynamics simulations performed on anisotropic Cu-Ni multilayers (Ghoniem and Han, 2005).

Similar behavior is also observed in dislocations penetrating through grain boundaries. For this case, the work done by the RSS on the dislocation needs to be greater than the combined energies of the grain boundary and the dislocation debris at that boundary (Li et al., 2009). Depending on the misorientation angle between the adjacent grains, the strength required for a dislocation to penetrate through the grain boundary was reported to be about 12.5 times the bulk strength, for very small misorientation angles, up to 200 times the bulk strength for large angles (Hasson and Goux, 1971; de Koning et al., 2002; Li et al., 2009).

In lieu of such observation, a range of barrier strengths were considered in order to examine the effects parametrically. Two limiting cases are addressed, namely a free surface case, $\sigma_c/\sigma_b = 0$, and a completely rigid barrier $\sigma_c/\sigma_b = \infty$. In addition to these limiting cases, two intermediate strengths are also studied, namely, $\sigma_c/\sigma_b = 15$, and 30, respectively. For Ni single crystals, the bulk strength is equal to $\sigma_b = 50$ MPa as reported from experiments (Dimiduk et al., 2005), and previous DD simulations (El-Awady et al., 2009).

Han and Ghoniem (2005); Akarapu and Zbib. (2009) developed analytical technique to compute the image forces on a dislocation near the interface between two bounded materials. It was shown that the image forces are of significance when the dislocation is within 10-20 atomic planes from the interface. Moreover, the maximum image stress a dislocation would sense is

precisely at the interface. In addition to other resistive forces arising from structural effects of the interface, this is what composes the Koehler barrier strength. Since the dimension of our simulation volumes are much larger than the zone affected by the image field, as a first approximation we truncate the image field to the interface where the maximum image stress (i.e. Koehler barrier strength) is applied.

In the following, in Sections 3.1 and 3.2 we first discuss the effect of the barrier strength on solid, and annular micropillars, respectively, without the activation of cross-slip. We then discuss the effect of the activation of cross-slip on the results, in Section 3.3.

3.1. Solid micropillars

The stress-strain relationships, without cross-slip activation, for solid micropillars having sizes $D = 0.25$, 0.5, 0.75, and 1.0 μm, are shown in Figure 2. For each size, the effect of varying the barrier strength, while the initial dislocation microstructure remains the same, is observed. Both the flow strength, as well as the hardening rate, increases with the increase in the barrier strength, σ_c. In the range of sizes simulated here, for a barrier strength of $\sigma_c/\sigma_b = 15$, the flow strength at 0.5% strain, increases by $30 - 50\%$ from simulations with free surface boundary conditions. In addition, for a barrier strength of $\sigma_c/\sigma_b = 30$, the flow strength at 0.5% strain, increases by $50 - 70\%$.

The hardening is also affected by the barrier strength. For the lower barrier strength, large strain bursts initiate at smaller strains and stresses. These strain bursts are associated with dislocation instabilities in the crystal, and arise from the collective, avalanche-like motion of the dislocations. This

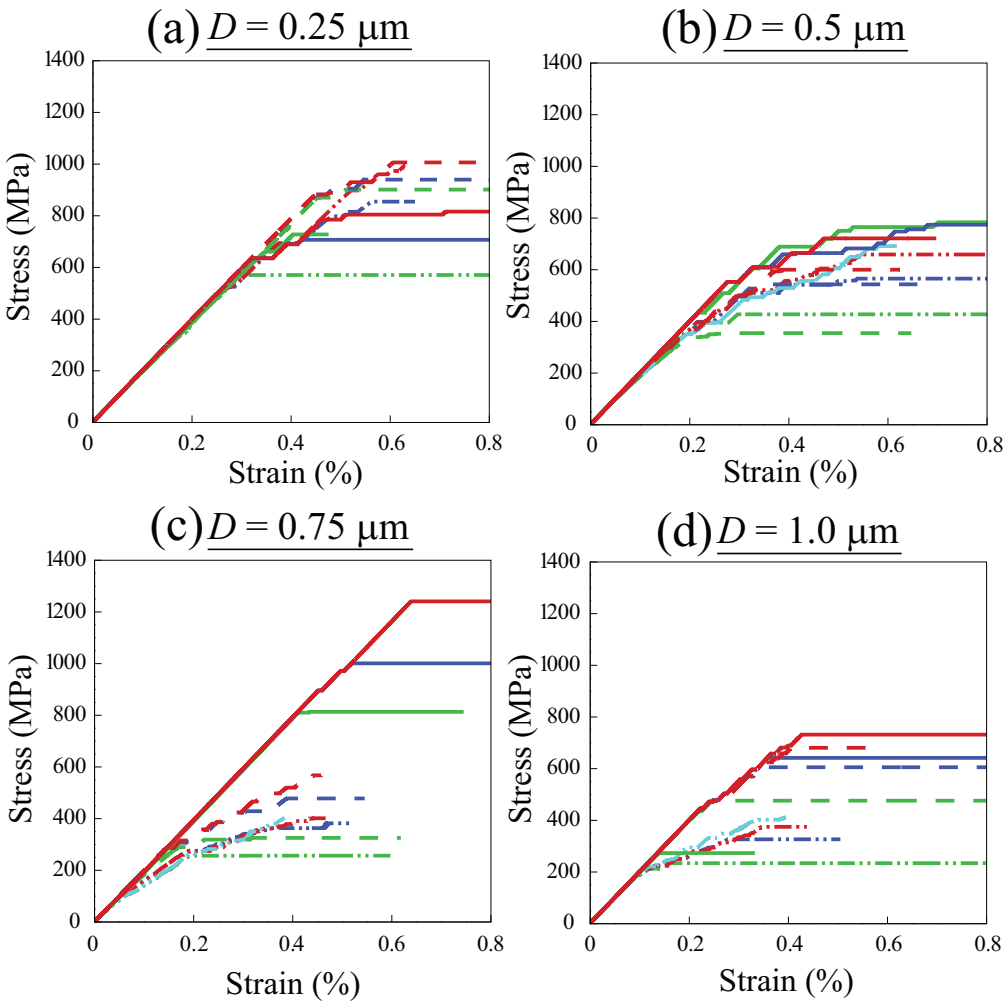

Figure 2: The computed stress-strain relationship of four solid cylindrical micropillars having sizes: (a) $D = 0.25$ μm; (b) $D = 0.5$ μm; (c) $D = 0.75$ μm; and (d) $D = 1.0$ μm. For each size, the initial dislocation microstructure is the same with the different barrier strength simulations. The green lines are free surface simulations, blue lines are simulations with $\sigma_c/\sigma_b = 15$, red lines are simulations with $\sigma_c/\sigma_b = 30$, and cyan lines are for fully impenetrable rigid surfaces. Solid lines, dashed lines, and dash dot dot lines are for simulations with "Case 1", "Case 2", and "Case 3" initial dislocation densities, respectively.

avalanche-like motion is attributed to the rise in the local stress state that may lead to the destruction of jammed dislocation configurations. As the barrier strength increases, the initiation of these large strain bursts are delayed to higher strain and stress regimes. In addition, as the barrier strength increases the magnitude of the strain bursts decreases, which results in a generally smoother stress-strain relationship. This can be observed for the infinitely rigid surface simulations.

From Figure 2, it is clear that for each micropillar size the response of the free surface simulations with the different initial dislocation densities varies. This is in accordance with previous simulation results that show that varying the source size distribution can lead to as much as 200-300% change in the flow strength for each pillar size (Rao et al., 2008; El-Awady et al., 2009). It is also observed that the magnitude of the effect of the presence of a strong barrier depends on the initial distribution of dislocations in the crystal. In the presence of a strong barrier, the evolving microstructure (i.e., dislocation speed and shape) would change. Thus, dipoles/junctions that could have formed in the absence of the strong barrier, may be instead avoided, and vice versa. This could have a significant effect on the flow strength response especially for the smaller crystals that have low initial dislocation densities, and thus the available sources in the crystal are scarce. This is evident in Figure 2 for simulations of pillar sizes $D = 0.25$ and 0.5 μm with the lowest initial dislocation density (Case 1).It is observed that the flow strength in these cases is higher for simulations with free surfaces than with a strong interface. This is because a junction that has formed in the free surface simulation was avoided in the strong barrier simulations. Thus, a higher

applied stress was required to break this junction since there were no other sources that could be activated at a lower strength. In the strong barrier simulations this junction was avoided and the dislocations had to overcome the barrier which had a lower strength than the junction. On the other hand, for larger crystals or at higher dislocation densities, the crystal would have a larger number of sources available to sample from. Thus, even if a junction forms, the next available source will be activated at a lower strength rather than breaking the junction.

In Figure 3, the dislocation density evolution of these micropillars are shown as a function of the barrier strength. In the simulations with free surfaces, the dislocation density is observed to increase slightly to a steady state value due to dislocations multiplication, surface truncation and escape from the pillar. On the other hand, for simulations with strong barriers, the dislocation density is observed to increase rapidly by an order of magnitude higher than for simulations of micropillars having free surfaces.

In Figure 4, the microstructure of a $D = 1.0$ μm solid pillar at 0.5% strain is shown. The barrier strength was $\sigma_c/\sigma_b = 15$, and the initial dislocation density was that of "Case 2". In simulations of micropillars larger than a few hundreds of nanometers having free surfaces, the dislocation sources are mostly single ended sources. We observe that the flow strength is mainly controlled by the weakest-link available in the system, which is bounded by the radius of the pillar. In addition, the exhaustion of such sources is attributed to junction formation and the activation of cross-slip, which is consistent with previous studies (Parthasarathy et al., 2007; Rao et al., 2008; El-Awady et al., 2008, 2009).

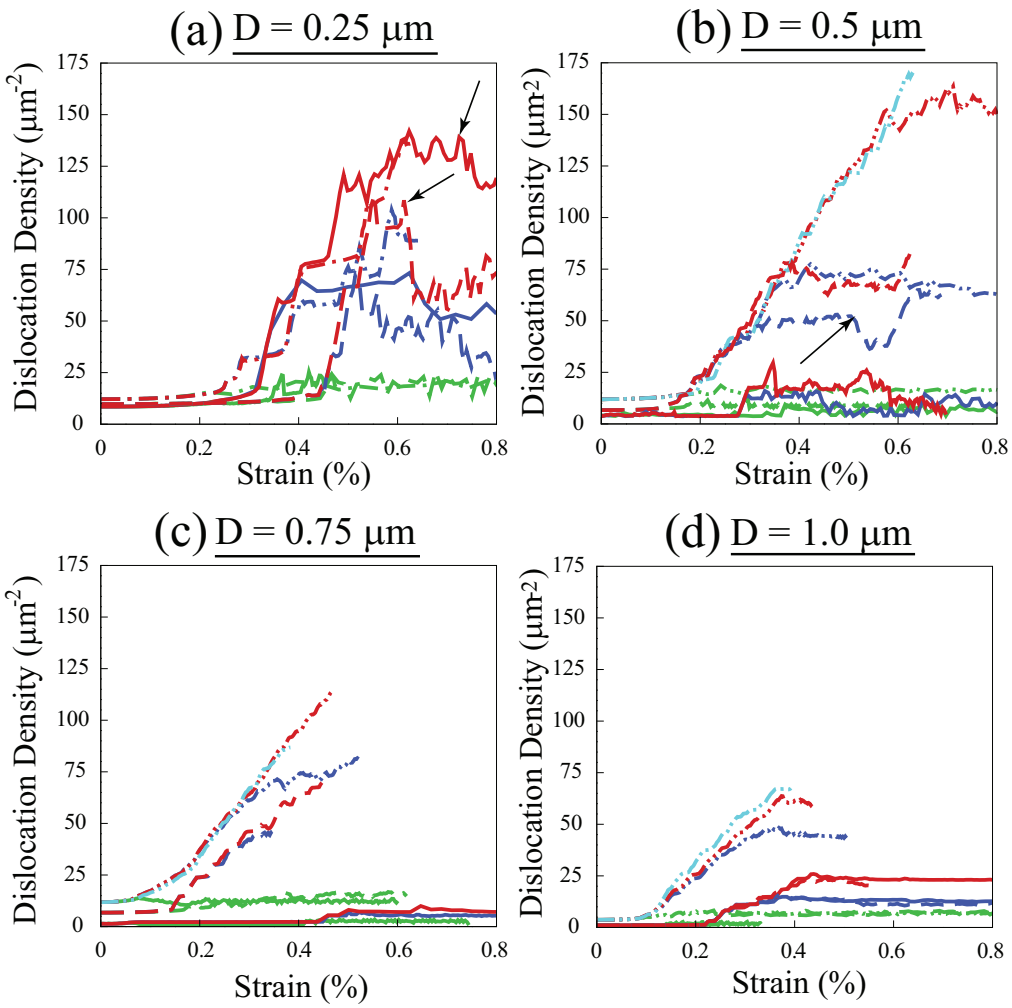

Figure 3: The dislocation density-strain relationship of four solid cylindrical micropillars: (a) $D = 0.25$ μm; $D = 0.5$ μm; $D = 0.75$ μm; $D = 1.0$ μm. For each size, the initial dislocation microstructure is the same with the different barrier strength simulations. The green lines are free surface simulations, blue lines are simulations with $\sigma_c/\sigma_b = 15$, red lines are simulations with $\sigma_c/\sigma_b = 30$, and cyan lines are for fully impenetrable rigid surfaces. Solid lines, dashed lines, and dash dot dot lines are for simulations with "Case 1", "Case 2", and "Case 3" initial dislocation densities, respectively. The arrows point at instances when weak spots have formed at the barrier.

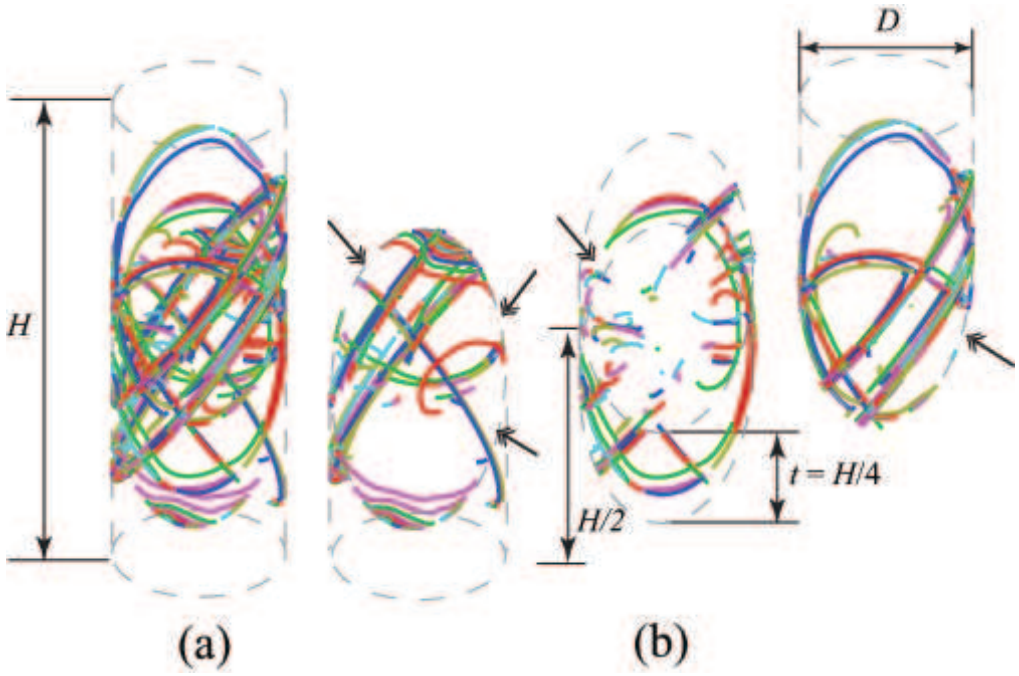

Figure 4: The microstructure at 0.5% strains of a $D = 1.0$ μm solid pillar having a barrier strength $\sigma_c/\sigma_b = 15$: (a) full 3-D view; and (b) cross-sectional views. The two headed arrows point at weak spots formed at the barrier.

For coated micropillars, as the weakest-links are first activated, some will be quickly exhausted due to junction formation, or trapped at the strong barrier, while the rest of the activated sources will continue to deposit additional dislocations at the strong barrier. This leads to dislocation pileups at the barrier, which exert an increasing back-stress on the operating sources. Eventually this back-stress leads to the complete shutdown of the active sources. This processes coincides with the formation of a small strain burst that is generally less than 0.05% strain. The pillar then deforms elastically until the increasing applied load can aid in overcoming the back-stresses and activate

additional sources, or until the local RSS exceeds the barrier strength. This latter event would then allow the leading dislocation to locally penetrate the barrier (i.e. cracking the barrier) and escape the pillar leaving a surface step. This is represented in our simulations by setting the barrier strength to zero on the local slipped region on the slip plane where the dislocation has escaped. This initiates a local weak spot from which subsequent dislocations can escape (see the two headed arrows in Figure 4). As a dislocation expands towards a weak spot on its slip plane, only a length of that dislocation equal to the length of the weak spot will be able to escape the pillar. The remainder length of the dislocation will be trapped at the stronger barrier that surrounds the weak spot as can be seen in Figure 4. Thus, more dislocations will pileup, which would result in increasing the local RSS and forming more weak spots on the slip plane. These weak spots will then interconnect in an unzipping manner along the surface of the pillar resulting in a large strain burst associated with a sudden drop in the dislocation density (see arrows in Figure 3). If and when the dislocations escaping through these weak spots are completely exhausted, further increase in the applied load is required to activate other sources and create additional weak spots. This produces a ladder-like hardening behavior.

When the barrier strength is relatively low, (e.g. $\sigma_c/\sigma_b = 15$), these weak spots initiate with a relatively large size and are dispersed at different locations on the surface of the pillar. This leaves wide gaps in the barrier, from which dislocations trapped inside the pillar can escape, and thus leads to larger strain bursts. On the other hand, when the barrier strength is relatively higher, (e.g. $\sigma_c/\sigma_b = 30$ and higher), when these weak spots initiate,

they are much smaller in size, and thus the strain bursts produced are much smaller. Only when the applied load is high enough, these smaller weak spots will interconnect or propagate in an unzipping manner, leading to a catastrophic flow event manifested in a large strain burst. The experimentally observed dependency of a smooth versus jerky stress-strain relationship as a function of the coating thickness (i.e. strength) reported by Ng and Ngan (2009), can be attributed to this difference in the initiation and propagation of the weak spots.

3.2. Annular micropillars

The effect of the barrier strength, without cross-slip activation, on the response of three annular micropillars is shown in Figure 5. The external diameter of all pillars is $D = 1.0$ μm, and the internal diameters are $D_i = 0.5$, 0.25, and 0.1 μm, respectively. Different boundary conditions were examined, with the internal and/or external surfaces simulated with a strong barrier and free surfaces. Similar to the results of solid micropillars, it is observed that increasing the barrier strength results in a stronger pillar. In addition, annular micropillars simulated with an external barrier only are observed to be stronger than the same annular micropillar with only an internal barrier. Also, for simulations with both internal and external barriers, the pillar flow strength is even higher.

The strengthening appears to be proportional to the "hard"surface to volume ratio. When this ration is small, the effect of the strengthening is observed to be minimal. On the other hand, when the hard surface to volume ration is large, the effect of strengthening can be substantial. As observed in Figure 5 for an annular pillar with internal diameter 0.5 μm, the flow

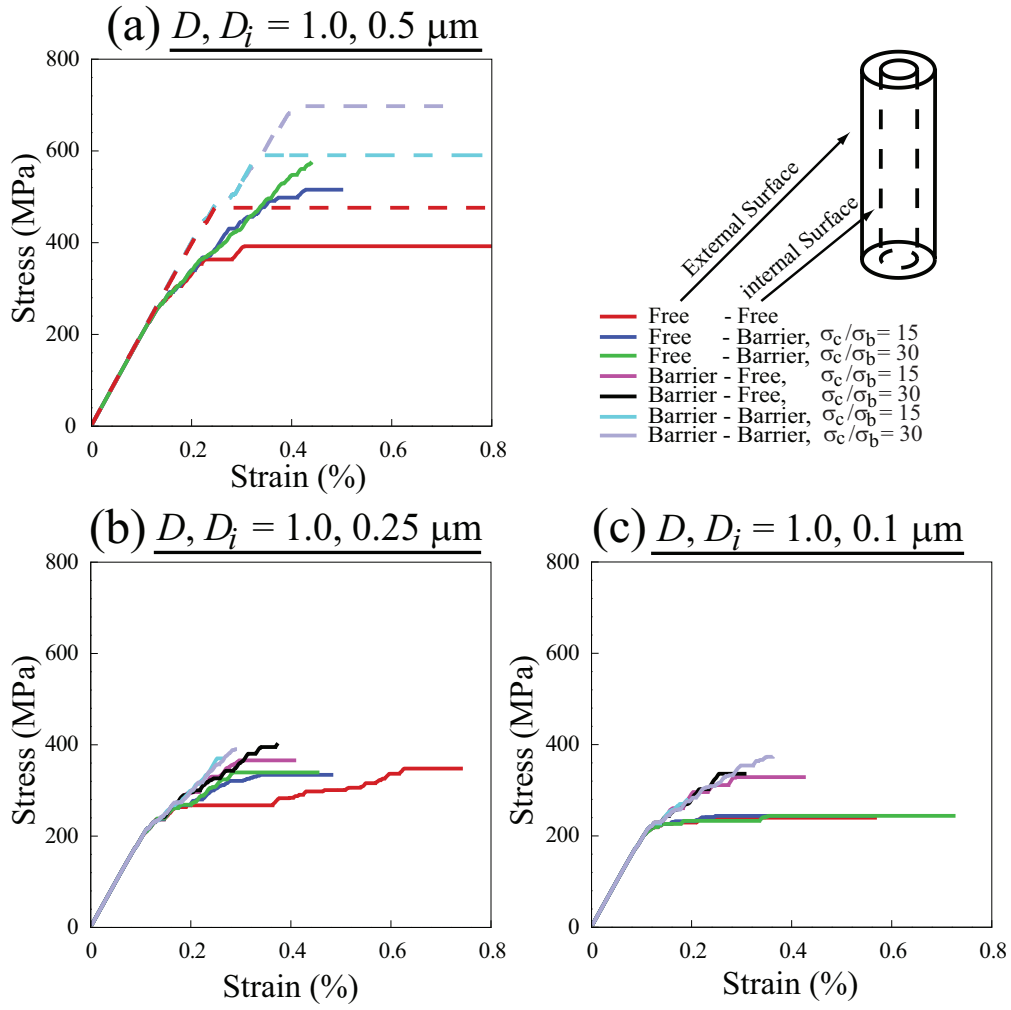

Figure 5: The stress-strain relationship of three annular pillars having an external diameter $D = 1.0$ μm and internal diameter: (a) $D_i = 0.5$ μm; (b) $D_i = 0.25$ μm; and (c) $D_i = 0.1$ μm. For each size, the initial dislocation microstructure is the same for the different barrier strengths simulated. Dashed lines are for "Case 1" simulations, and solid lines are for "Case 2" simulations.

strength at 0.5% strain can increase by up to 50%, compared to the same annular pillar simulated with a free-surface boundary conditions. On the other hand, for an internal diameter of 0.1 μm, the strengthening is only a few percent higher. This difference may be attributed to two boundary effects produced by the larger hard surface to volume ratio, first the sources in these pillars are much smaller due to the smaller volume, and second more dislocations get trapped due to the large hard surface area.

This is evident from the dislocation density evolution shown in Figure 6 where the densities shown here are for the same micropillars discussed in Figure 5. The effect of a strong internal barrier is observed to be dependent on the internal diameter, D_i. As D_i increases, more dislocations are trapped at the internal barrier, and the dislocation density increases. For the case with $D_i = 0.5$ μm, the dislocation density can increase by 10 to 20 times, depending upon the barrier strength, compared to those in the same annular pillars having free-surface boundary conditions. For the annular pillars with a much smaller internal diameter, $D_i = 0.1$ μm, the dislocation density does not change much from simulations with free-surfaces. This is because the internal surface is small and only a small number of dislocations will be trapped at that barrier, thus minimally affecting the plasticity of these pillars. On the other hand, the effect of an external barrier is independent of the internal diameter. The presence of an external barrier is observed to increase the dislocation density by 15 to 20 times from simulations with free-surfaces.

The effect of the internal diameter on the microstructure evolution in annular pillars with free surfaces is shown in Figure 7. The two pillars have

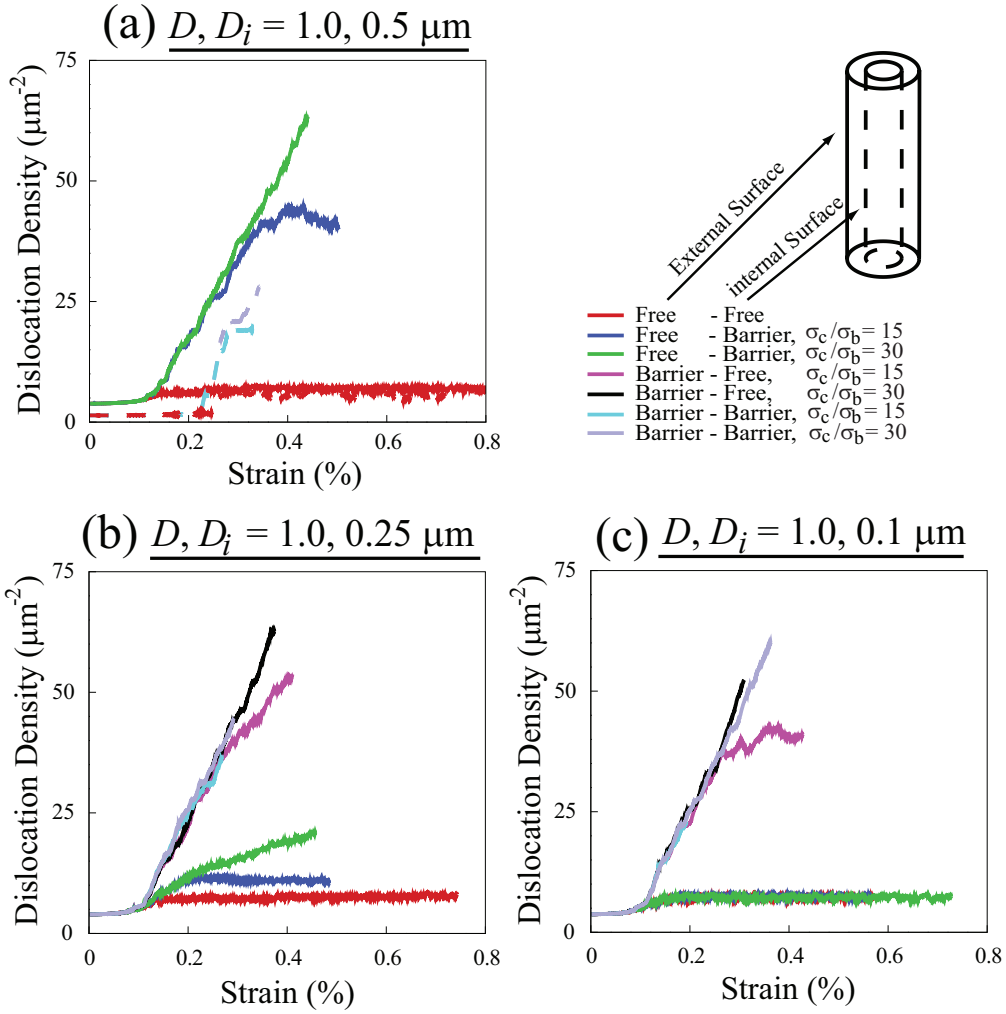

Figure 6: The dislocation density-strain relationship of three annular pillars having an external diameter $D = 1.0$ μm and internal diameter: (a) $D_i = 0.5$ μm; (b) $D_i = 0.25$ μm; and (c) $D_i = 0.1$ μm. For each size, the initial dislocation microstructure is the same for the different barrier strength simulations. Dashed lines are for "Case 1" simulations, and solid lines are for "Case 2" simulations.

an external diameter $D = 1.0$ μm and internal diameters $D_i = 0.5$, and 0.1 μm, respectively. The initial microstructure is that of "Case 2". As dislocation sources are activated, they expand and terminate at either the internal or external surfaces. This will generate new single ended sources that are either of an equivalent or shorter lengths. As these new sources are further activated, they will expand and terminate at the other free surface. Thus producing threading dislocations that span the length between the two free surfaces. This is similar to the microstructure observed in thin metal films (Nix, 1998).

Figure 8 shows the effect of the barrier strength on the microstructure evolution of the same two pillars discussed in Figure 4. In Figure 8-a, only the external surface has a barrier strength of $\sigma_c/\sigma_b = 15$, while the internal surface is free. In Figure 8-b both the internal and external surfaces have a barrier strength of $\sigma_c/\sigma_b = 30$. It is clear that more dislocation are trapped at the external surface barrier when the barrier strength is higher ($\sigma_c/\sigma_b = 30$). In addition, in the annular pillar with the small internal diameter of $D_i = 0.1$ μm, although the internal surface has a barrier with a high strength, only a small number of dislocations are trapped at that surface verses those trapped at the outer surface. As more dislocations are activated due to the increase in the applied load, more dislocations pileup at the surface barriers, and thus increase the back-stress on the leading dislocations at the surface barrier. When this stress locally exceeds the barrier strength, the leading dislocation will break through the barrier, leaving a week spot from which subsequent dislocations can escape from.

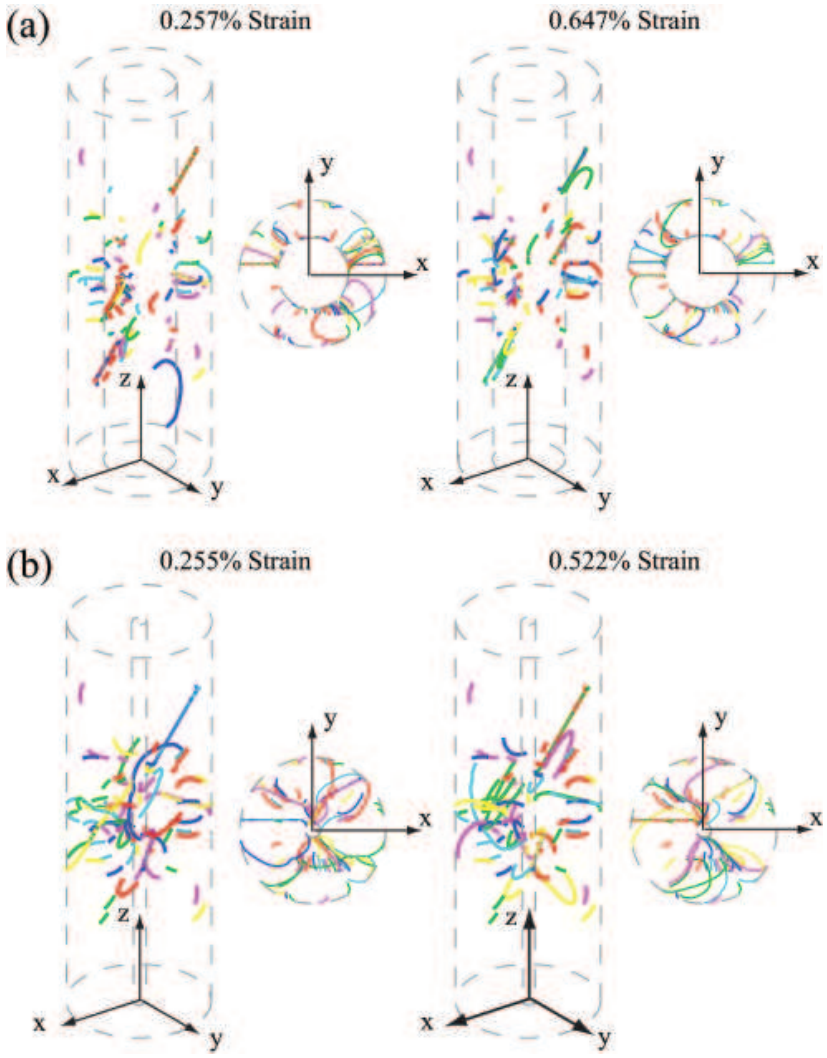

Figure 7: Comparison between the microstructure evolution of two simulated annular pillars. Both annular pillars having an external diameter $D = 1.0$ μm. In (a) the microstructure for an internal diameter of $D_i = 0.5$ μm, is shown at 0.257%, and 0.647% strain, respectively. In (b) the microstructure for an internal diameter of $D_i = 0.1$ μm, is shown at 0.255%, and 0.522% strain, respectively. Both internal and external surfaces are simulated as free surfaces.

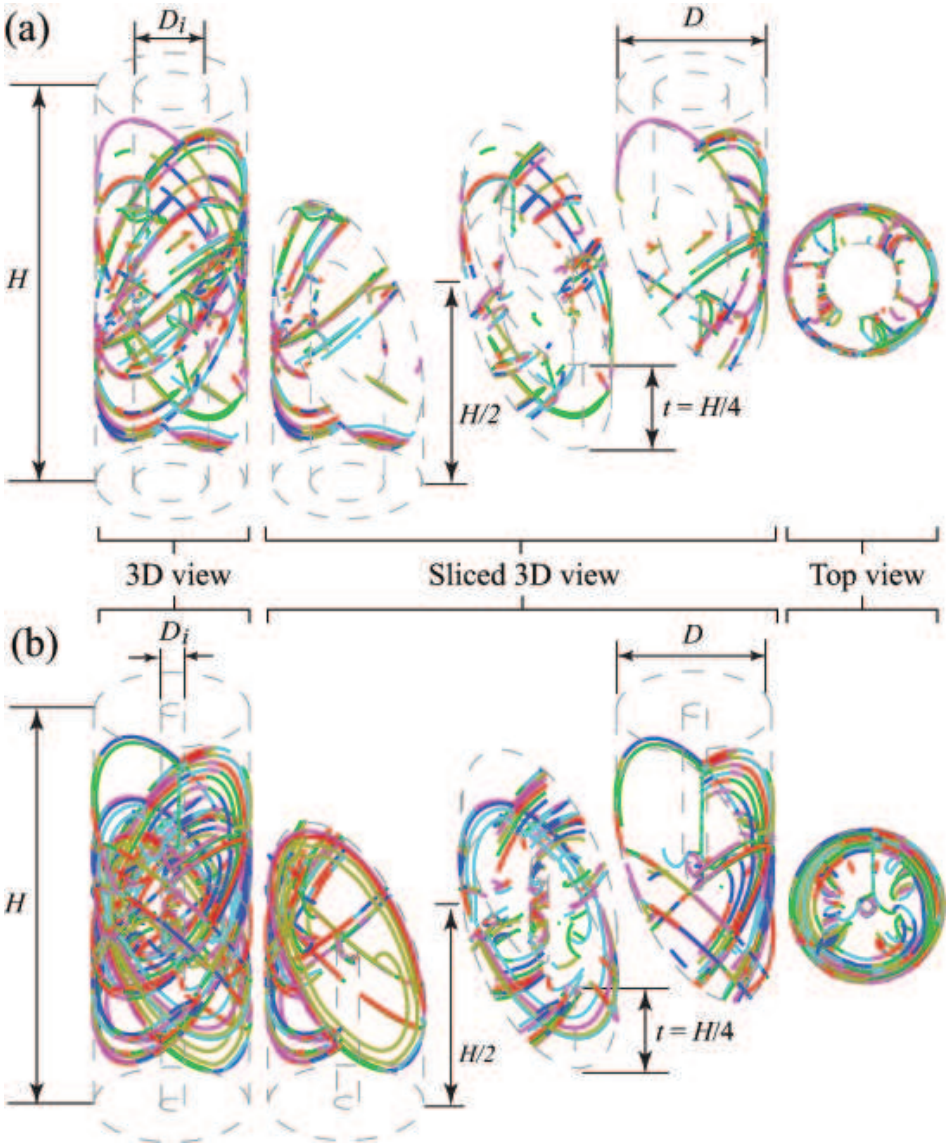

Figure 8: The effect of the barrier strength on the microstructure evolution of two simulated annular pillars having $D = 1.0$ μm and: (a) $D_i = 0.5$ μm, external surface barrier strength $\sigma_c/\sigma_b = 15$, and a free internal surface; (b) $D_i = 0.1$ μm and an external and internal surface barrier strengths of $\sigma_c/\sigma_b = 30$.

3.3. Effects of cross-slip activation

Dislocation cross-slip is generally associated with several aspects of macroscopic materials deformation. In addition to controlling stage-III work-hardening in bulk materials, cross-slip is also associated with substructure morphology and evolution. On the other hand, at the micron and submicron scales, cross-slip activation and its effects is still under debate (Lee and Nix, 2010). A number of recent 3DD simulations have discussed the importance and effects of cross-slip on the plasticity of micropillars (El-Awady et al., 2009; Motz et al., 2009; Zhou et al., 2009). In all DD simulations, cross-slip activation is based on a stochastic probabilistic model (Kubin et al., 1992). Further details about this model probabilistic model within our current PDD framework can be found elsewhere (El-Awady et al., 2009).

In Figure 9, a comparison between the stress-strain response with and without cross-slip activations is shown for three solid micropillars of sizes $D = 0.5$, 0.75, and 5.0 μm, and one annular pillar with $D = 1.0$ μm and $D_i = 0.5$ μm. The results are shown for barrier strengths $\sigma_c/\sigma_b = 15$, and $\sigma_c/\sigma_b = 30$. It is observed that for smaller pillars $D < 1.0$ μm, the strength of the pillars drops by about 10% for simulations with cross-slip activation versus simulations without cross-slip activation. This is true for both solid and annular micropillars. On the other hand, for the larger pillar simulation (i.e. $D = 5.0$ μm) cross-slip activation was observed to have the reverse effect.

This can be explained as follows. For smaller pillars having low dislocation densities (in the range of 10^{12} to 10^{13} m^{-2}) the number of sources available in the pillar are limited (Rao et al., 2008; El-Awady et al., 2009). As the applied

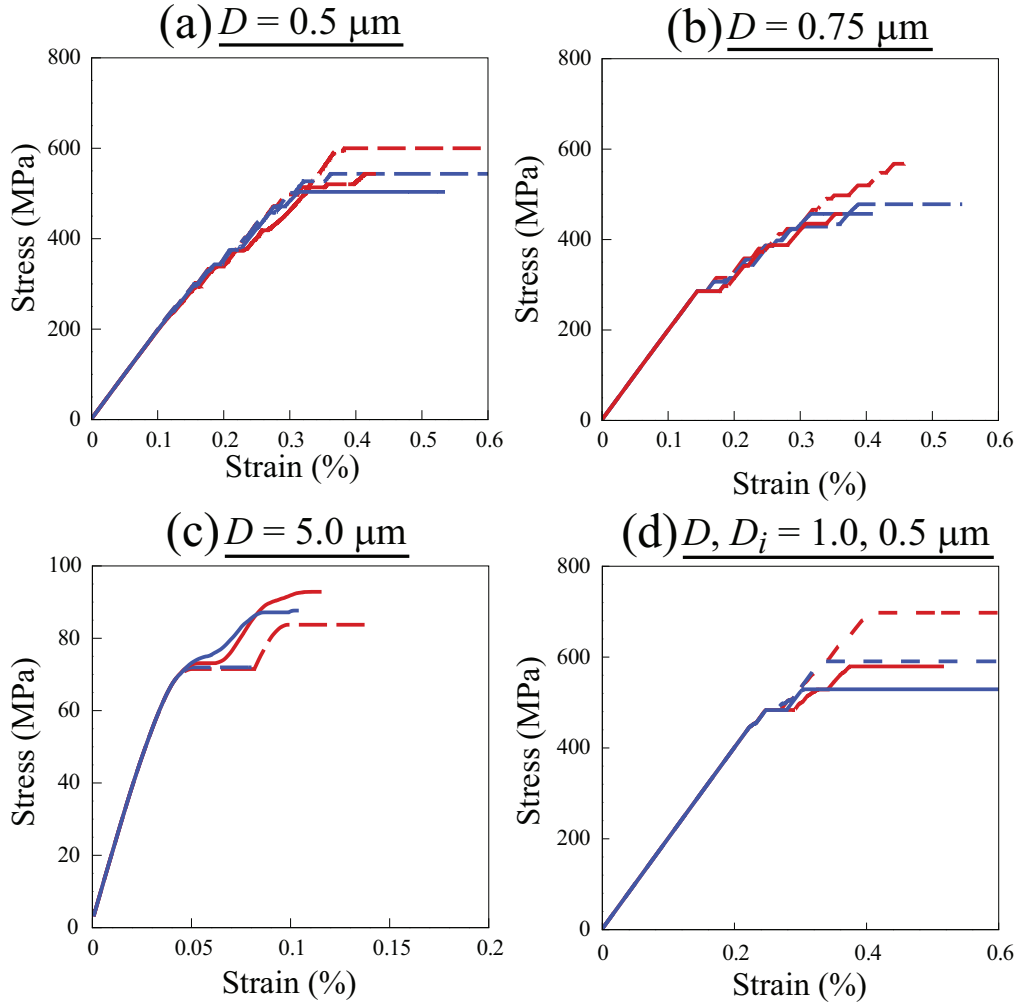

Figure 9: Comparison between the stress-strain response with and without cross slip activation of: (a) $D = 0.5$ μm solid micropillar; (b) $D = 0.75$ μm solid micropillar; (c) $D = 5.0$ μm solid micropillar; and (d) $D = 1.0$ μm and $D_i = 0.5$ μm annular micropillar. Solid and dashed lines are for simulations with, and without cross-slip activation, respectively. The external and internal surfaces were assumed to have barrier strength $\sigma_c/\sigma_b = 15$ (blue lines), and $\sigma_c/\sigma_b = 30$ (red lines).

load increases and these sources are activated, dislocations will pileup at the strong barrier. As the back stress builds up, screw dislocations close to the barrier will then have a high probability of cross-slipping to an equivalent slip plane. This has the effect of carrying the plastic flow to planes on which the dislocation can freely glide without the need to increase the applied load further. The flow strength of these small micropillars will thus be lower than equivalent pillars when cross-slip is not considered.

This can be clearly observed from the microstructure at 0.4% of an annular pillar with $D = 1.0$ μm and $D_i = 0.5$ μm shown in Figure 10. Both the internal and external surfaces have a barrier strength of $\sigma_c/\sigma_b = 15$. In Figure 10-a, no cross slip activation was included and it is clear that dislocation activation is limited to a small number of planes. Thus, higher stresses are required for the dislocations to penetrate through the strong barrier. On the other hand, in Figure 10-b cross-slip activation was included and it is clear that dislocations have cross-slipped to other slip systems were they can glide on more freely.

On the other hand, for the larger pillar simulations, more dislocation sources are available in the pillar. With the activation of cross-slip, the continuous propagation and trapping of dislocations at the strong barrier will result in an inhomogeneous dislocation accumulation. Such an inhomogeneous dislocation accumulation leads to the development of slip bands that would create new internal barriers and affect the flow strength of the crystal (Wang et al., 2009). In the smaller crystals this inhomogeneous dislocation accumulation is less severe since the number of dislocation sources is limited. Thus, slip bands are less likely to be developed. In Figure 11, the microstruc-

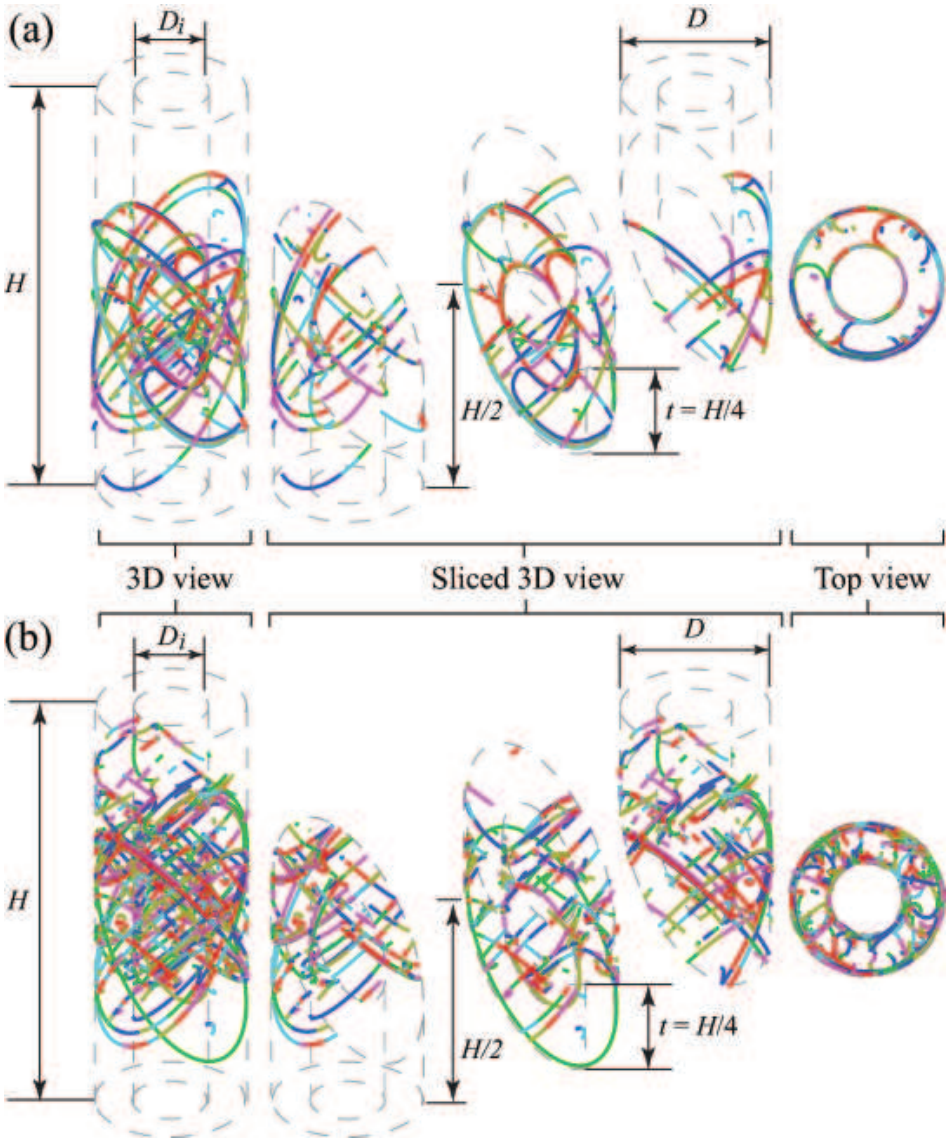

Figure 10: Comparison between the microstructure at 0.4% strain of an annular pillar of size $D = 1.0$ μm and $D_i = 0.5$ μm: (a) without cross-slip activations; and (b) with cross-slip activation.

ture at 0.1% strain of $D = 5.0$ μm solid micropillar is shown. The external surface has a barrier strength of $\sigma_c/\sigma_b = 30$. With cross-slip, we observe dislocations moving to other glide planes, and sometimes double-cross slipping, producing a thickening of the slip traces at the surface (consistent with experimental observations (Dimiduk et al., 2005; Norfleet et al., 2008)). In Figure 11, we capture elements of this process by plotting dislocations above or below the slip planes of the original sources. In simulations without cross-slip, dislocations are not observed running parallel to the original activated slip planes.

4. Discussion and Conclusions

The observations from the current simulation results on both solid and annular micropillars are consistent with experimental observations of coated/centrally-filled micropillars with similar sizes performed by Ng and Ngan (2009). From the experimental results, it was observed that for solid pillars of size $D = 1.2$ μm, as the external coating thickness increases (i.e. stronger barrier strength), the stress-strain relationship is generally smoother due to much smaller strain bursts. On the other hand, for thin coatings (i.e. weak barrier strength), the stress-strain behavior is jerky-like and similar to monolithic pillars. The strengthening effect of the coatings was observed for both thin as well as thick coatings, and the flow strength at 2% strain can reach up to 80% higher than that of coat-free micropillars. From the current simulations, the flow strength at 0.5% strain was observed to increase by $30 - 70\%$ depending on the barrier strength. In addition, for a lower barrier strength, large strain bursts initiate at smaller strains and stresses. As the barrier

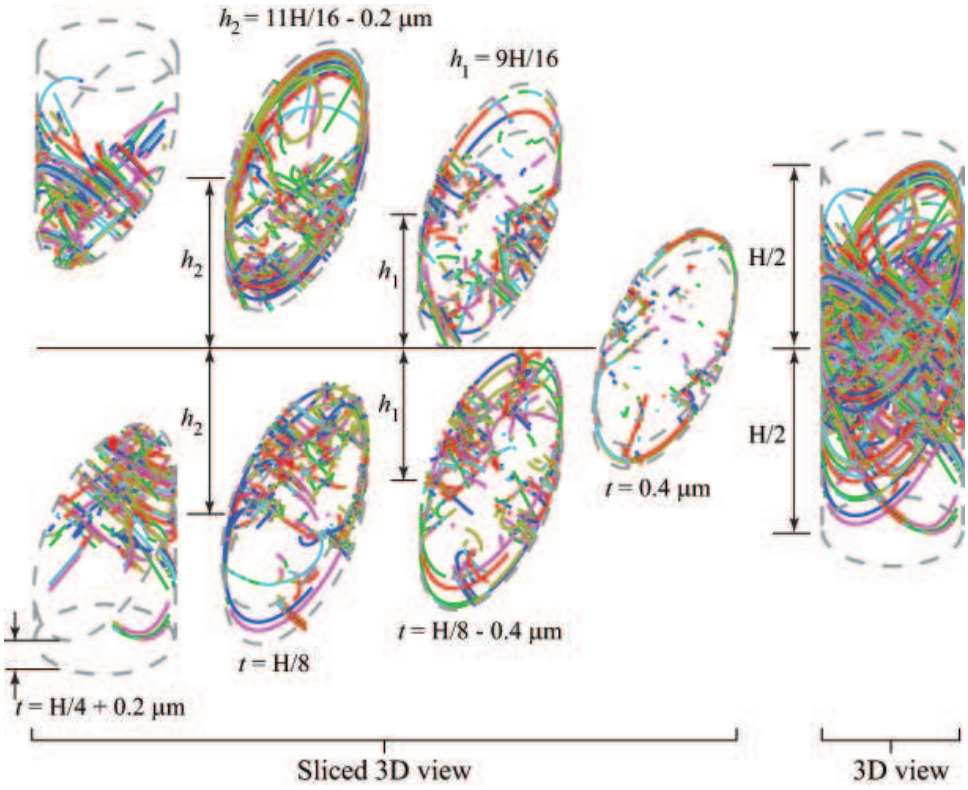

Figure 11: The microstructure of a $D = 5.0$ μm solid micropillar at 0.1% strain with the activation of cross-slip. Thickening of the slip traces at the surface is observed in the sliced 3D view.

strength increases, the initiation of these large strain bursts are delayed to higher strain and stress regimes and their magnitude decreases, which results in a generally smoother stress-strain relationship.

On the other hand, from the experiments, for center-filled pillars with an outer diameter $D = 1.2$ μm and internal diameters in the range $D_i = 0.3$ to ~ 0.5 μm, the flow strength at 2% strain was shown to be $\sim 30 - 200\%$ larger than filling-free annular pillars with similar internal diameter. In

addition, similar to the current simulation observations, it was also observed that annular pillars that have been both center-filled and externally coated were stronger than the same annular center-filled pillars alone. From the current simulations of annular pillars with an internal strong barrier, the flow strength at 0.5% strain is observed to increase by up to 50% compared to the same annular pillar simulated with free-surface boundary conditions.

It should be mentioned here that, the current simulations are different than the experiments performed on centrally-filled micropillars (Ng and Ngan, 2009). In the experiments, these centrally-filled annular pillars are in fact solid pillars made up from two materials. Thus, these experiments involve the compression of an annular pillar fabricated from a softer material along with the compression of the deposited stronger material in the shape of a solid pillar having an external diameter equal to the internal diameter of the annular material. On the other hand, in the current simulations, only a monolithic annular pillar with hard surfaces is compressed. This may explain the much stronger effects observed experimentally with central-fillings versus the current simulation results.

Annular micropillars clearly exhibit a size effect similar to that observed in solid micropillars. In previous work on solid micropillars, it was shown that the radius of the pillar is the limiting parameter for the length of the activated dislocation sources (Parthasarathy et al., 2007; El-Awady et al., 2009). In addition, the flow strength versus pillar diameter was shown to follow a power law with an exponent that has been computed experimentally and computationally to be in the range -0.4 to -1.0 (Rao et al., 2008; Uchic et al., 2009).

In Figure 12, a composite plot of the flow strength versus the micropillar diameter for the current simulation results of solid and annular Ni micropillars, in addition to the experimental results on Al coated and centrally filed micropillars (Ng and Ngan, 2009). These data are superimposed on a shaded area representing all the experimental and simulation results on solid micropillars as reported by Uchic et al. (2009). The flow strength is normalized by the shear modulus and the Burgers vector of each material. Clearly, the current results for solid and annular pillars, with and without a strong barriers, fall within the same range of results of previous work on monolithic micropillars.

A number of observations can be made about the results shown in Figure 12. The flow strength is typically computed at 2% strain for experimental results. On the other hand, in 3-D DD simulations, due to the computational complexity of simulations over 1% strain, the flow strength is typically computed in the range 0.5-1% strain. Thus, additional strain hardening that can occur in the experiments at higher strains might not be represented by simulation results. This is especially true for larger pillars, $D \geq 5.0$ μm, where excessive forest hardening can take place as was discussed in Section 3.3. This in addition to the fact that the initial dislocation density in the experiments on the largest pillars is already an order of magnitude higher that used in the current simulations. These observations can explain the excessive hardening observed experimentally for the largest coated pillars, at 2% strain, which is about 200%, versus only 20% hardening, at 0.15% strain, for the current simulations on similar sized micropillars.

Also, it should be noted that the annular micropillars flow strength data

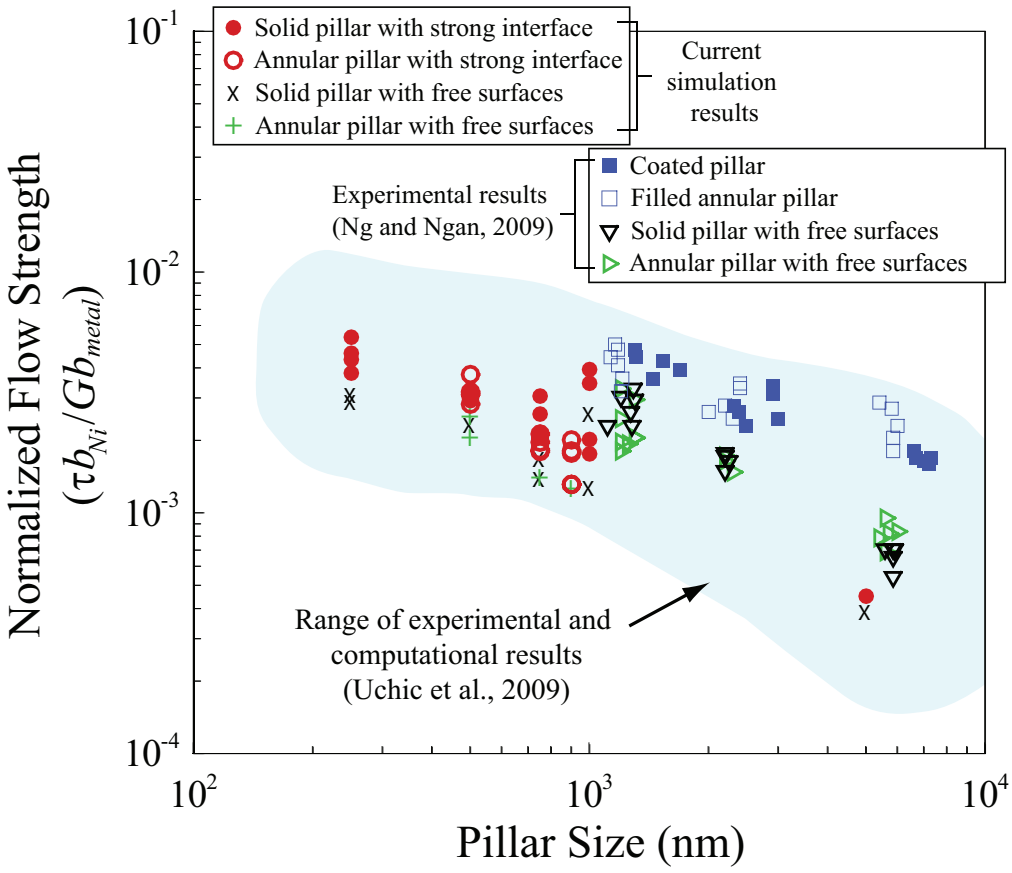

Figure 12: The flow strength versus micropillar size for the current simulations of solid and annular Ni micropillars, in addition to the experimental results of coated and center-filled Al pillars by Ng and Ngan (2009). Flow strength data are normalized by the shear modulus and the Burgers vector of each material. For the simulated annular pillars, the effective diameter, $D_{eff} = (D - D_i)$, is used as the size of the pillar, while for all other cases, the external diameter is used. The shaded area represents the range of experimental and computational results as reported by Uchic et al. (2009).

fall within the cloud of experimental and computational data obtained for solid pillars. In addition, similar to observations on solid micropillars, large scatter is observed from annular pillars results of the same size. It was reported by El-Awady et al. (2009) that because of such huge scatter the correlation between the flow strength and the pillar diameter is not strong. Instead, a stronger correlation was obtained relating the flow strength to the average length of the activated dislocation sources. This relationship is a power law, with an exponent in the range -0.79 to -0.89 (El-Awady et al., 2009). For the solid pillar having size $D = 1.0$ μm and initial dislocation density 3.7 $\times 10^{12}$ m^{-2}, the average activated dislocation length was, $\lambda = 0.216$ μm and the flow strength, at 0.5% strain, was 234.2 MPa. By carving annular pillars from this starting geometry with internal diameters of $D_i = 0.1$, 0.25, and 0.5 μm, the new average activated dislocation lengths were, $\lambda = 0.21$, 0.1637, and 0.1124 μm, respectively. The flow strength, at 0.5% strain, of these annular pillars was 239.94, 300.79, and 392.28 MPa, respectively. By using these data to compute the exponent relating these annular pillar flow strengths to the average length of activated dislocations, we get an exponent equal to -0.79. This is within the range of computed exponents of solid pillars (El-Awady et al., 2009). Thus, similar to solid pillars, it can be concluded that the size-effects observed for the annular pillars are consistent with the "weakest-link activation mechanism". Also, it should be noted that the upper limit on the weakest-link in annular pillars is the effective radius of the pillar, $R_{eff} = (D - D_i)/2$.

Another important point that can be concluded from the current results is the effect of the presence of an amorphous layer. This layer, if it exists,

can have a width in the order of tens of nanometers depending on the bulk material (McCaffrey et al., 2001). It also may act as a barrier to dislocation motion. As observed from the results presented in Figure 12, if such a layer would to exist, it might strengthen the pillar by up to 80% for solid micropillars. Since, the observed and calculated size strengthening for FCC metals is an order of magnitude larger than this, it can be concluded that even if an amorphous layer is present, its effect on strengthening of the micropillar is by no means a controlling factor in the observed size-dependance.

In summary, we have performed three-dimensional dislocation dynamics simulations of solid and annular pillars having free surfaces, and strong external and/or internal barriers. The annular pillars are shown to exhibit a similar size effect to that observed in solid pillars. The scaling observed is consistent with the weakest-link activation mechanism and depends on the effective pillar diameter, $D_{eff} = D - D_i$. The presence of an external strong barrier (or layer coating) is observed to dramatically increase the dislocation density by an order of magnitude due to trapping dislocations at the strong barrier. In addition, a considerable increase in the flow strength by up to 60% from simulations with free surface boundary conditions is observed. At lower barrier strengths, large dispersed weak spots are initiated as the applied stress increases, while for higher barrier strengths these weak spots are smaller and localize on a limited number of slip planes. This results in a relatively smoother stress-strain response at higher barrier strengths. In addition, the hardening rate is also observed to increase with increasing barrier strength. Finally the results are in qualitative agreement with recent compression experimental of coated and centrally filled micropillars.

Acknowledgements

This work was supported by the US AFOSR, and by a grant of computer time from the DOD High Performance Computing Modernization Program, at the Aeronautical Systems Center/Major Shared Resource Center.

References

Akarapu, S., Zbib, H.M., 2009. Line-integral solution for the stress and displacement fields of an arbitrary dislocation segment in isotropic bimaterials in 3D space. Phil. Mag. 89 (25), 2149–2166.

Akarapu, S., Zbib, H.M., D.F. Bahr, 2010. Analysis of heterogeneous deformation and dislocation dynamics in single crystal micropillars under compression. Int. J. Plasticity 26 (2), 239–257.

Baker, S., Keller-Flaig, R.-M., Shu, J., 2003. Bauschinger effect and anomalous thermomechanical deformation induced by oxygen in passivated Cu films on substrates. Acta Mater. 51 (10), 3019–3036.

Benzerga, A., Shaver, N., 2006. Scale dependence of mechanical properties of single crystals under uniform deformation. Scripta Mater. 54 (11), 1937–1941.

Benzerga, A., 2009. Micro-pillar plasticity: 2.5D mesoscopic simulations. J. Mech. Phys. Solids 57 (9), 1459–1469.

de Koning, M., Miller, R., Bulatov, V., Abraham, F., 2002. Modelling grain-boundary resistance in intergranular dislocation slip. Phil. Mag. A. 82 (13), 2511–2527.

Dimiduk, D., Uchic, M., Parthasarathy, T., 2005. Size-affected single-slip behavior of pure nickel microcrystals. Acta Mater. 53 (15), 4065–4077.

El-Awady, J. A., Biner, S. B., Ghoniem, N. M., 2008. A self-consistent boundary element, parametric dislocation dynamics formulation of plastic flow in finite volumes. J. Mech. Phys. Solids 56 (5), 2019–2035.

El-Awady, J. A., Wen, M., Ghoniem, N. M., 2009. The role of the weakest-link mechanism in controlling the plasticity of micropillars. J. Mech. Phys. Solids 57 (1), 32–50.

Espinosa, H., Panico, M., Berbenni, S., Schwarz, K., 2006. Discrete dislocation dynamics simulations to interpret plasticity size and surface effects in freestanding FCC thin films. Int. J. Plasticity 22 (11), 2091–2117.

Ghoniem, N., Han, X., 2005. Dislocation motion in anisotropic multilayer materials. Phil. Mag. 85, 2809–2830.

Ghoniem, N., Sun, L., 1999. Fast sum method for the elastic field of 3-D dislocation ensembles. Phys. Rev. B 60 (1), 128–140.

Ghoniem, N., Tong, S.-H., Sun, L., 2000. Parametric dislocation dynamics: A thermodynamics-based approach to investigations of mesoscopic plastic deformation. Phys. Rev. B 61 (2), 913–927.

Greer, J., Oliver, W., Nix, W., 2005. Size dependence of mechanical properties of gold at the micron scale in the absence of strain gradients. Acta Mater. 53 (6), 1821–1830.

Han, X., Ghoniem, N., 2005. Stress field and interaction forces of dislocations in anisotropic multilayer thin films. Phil. Mag. 85 (11), 1205–1225.

Hasson, G., Goux, C., 1971. Interfacial energies of tilt boundaries in aluminim. experimental and theoretical determination. Scr. Metall. 5, 889–894.

Kiener, D., Motz, C., Rester, M., Jenko, M., Dehm, G., 2007. FIB damage of Cu and possible consequences for miniaturized mechanical tests. Mater. Sci. Eng. A 459, 262–272.

Kubin, L., Canova, G., Condat, M., Devincre, B., Pontikis, V., Bréechet, Y., 1992. Dislocation microstructures and plastic flow: a 3-D simulation. Diffusion and Defect Data - Solid State Data, Part B (Solid State Phenomena) 23–24, 455–472.

Lee, S.-W., Han, S., Nix, W., 2009. Uniaxial compression of FCC Au nanopillars on an MgO substrate: The effects of prestraining and annealing. Acta Mater. 57 (15), 4404–4415.

Lee, S.-W., Nix, W., 2010. Geometrical analysis of 3D dislocation dynamics simulations of FCC micro-pillar plasticity. Mater. Sci. Eng. A. 527 (7-8), 1903–1910.

Li, Z., Hou, C., Huang, M., Ouyang, C., 2009. Strengthening mechanism in micro-polycrystals with penetrable grain boundaries by discrete dislocation dynamics simulation and hall-petch effect. Comp. Mater. Sci. 46 (4), 1124–1134.

Liu, X.H., Schwarz, K.W., 2005. Modelling of dislocations intersecting a free surface, Model. Simul. Mater. Sci. Eng. 13, 12331247.

Maaβ, R., Grolimund, D., Van Petegem, S., Willimann, M., Jensen, M., Van Swygenhoven, H., Lehnert, Gijs, M., Volkert, G., Lilleodden, E., Schwaiger, R., 2006. Defect structure in micropillars using x-ray microdiffraction. Appl. Phys. Lett. 89 (151905).

McCaffrey, J., Phaneuf, M., Madsen, L., 2001. Surface damage formation during ion-beam thinning of samples for transmission electron microscopy. Ultramicroscopy 87, 97–104.

Motz, C., Weygand, D., Senger, J., Gumbsch, P., 2009. Initial dislocation structures in 3-D discrete dislocation dynamics and their influence on microscale plasticity. Acta Mater. 57 (6), 1744–1754.

Ng, K., Ngan, A., 2009. Effects of trapping dislocations within small crystals on their deformation behavior. Acta Mater. 57 (16), 4902–4910.

Nicola, L., Van der Giessen, E., Needleman, A., 2003. Discrete dislocation analysis of size effects in thin films. J. Appl. Phys. 93, 5920–5928.

Nicola, L., Xiang, Y., Vlassak, J., Van der Giessen, E., Needleman, A., 2006. Plastic deformation of freestanding thin films: Experiments and modeling. J. Mech. Phys. Solids 54, 2089–2110.

Nix, W., 1998. Yielding and strain hardening of thin metal films on substrates. Scr. Mater. 39, 545–554.

Norfleet, D., Dimiduk, D., Polasik, S.J., a. U. M., Mills, M., 2008. Dislocation structures and their relationship to strength in deformed nickel microcrystals. Acta Mater. 56 (13), 2008.

Oh, S., Legros, M., Kiener, D., Dehm, G., 2009. In situ observation of dislocation necleation and escape in a submicrometer aluminium single crystal. Nat. Mater. 8, 95–100.

Parthasarathy, T., Rao, S., Dimiduk, D., Uchic, M., Trinkle, D., 2007. Contribution to size effect of yield strength from the stochastics of dislocation source lengths in finite samples. Scr. Mater. 56 (4), 313–316.

Rao, S., Dimiduk, D., Parthasarathy, T., Uchic, M., Tang, M., Woodward, C., 2008. Athermal mechanisms of size-dependent crystal flow gleaned from three-dimensional discrete dislocation simulations. Acta Mater. 56 (13), 3245–3259.

Rao, S., Hazzledine, P., 2000. Atomistic simulations of dilocation-interface interactions in the Cu-Ni multilayer system. Phil. Mag. A 80 (9), 2011–2040.

Rubanov, S., Muroe, P., 2004. FIB-induced damage in silicon. J. Microsc. 214 (3), 213–221.

Shade, P., Weeler, R., Choi, Y., Uchic, M.D., a. D. D., Fraser, H., 2009. A combined experimental and simulation study to examine the lateral constraint effects on microcompression of single-slip oriented single crystals. Acta Mater. 57 (15), 4580–4587.

Shan, Z., Mishra, R., Asif, S., Warren, O., Minor, A., 2008. Mechanical annealing and source-limited deformation in submicrometer-diameter Ni crystals. Nature Mater. 7, 115–119.

Shim, S., Bei, H., Miller, M., Pharr, G., George, E., 2009. Effects of focused ion beam milling on the compressive behavior of directionally solidified micropillars and the nanoindentation response of an electropolished surface. Acta Mater. 57 (2), 503–510.

Tang, H., Schwarz, K., Espinosa, H., 2008. Dislocation-source shutdown and the plastic behavior of single-crystal micropillars. Phys. Rev. Lett. 100 (185503).

Uchic, M., Dimiduk, D., Florando, J., Nix, W., 2003. Exploring specimen size effects in plastic deformation of Ni_3(Al,Ta). In: George, E. (Ed.), Materials Research Society Symposium Proceedings. Vol. 753. Materials Research Society, Pittsburgh, PA, pp. BB1.4.1.–BB1.4.6.

Uchic, M., Dimiduk, D., Florando, J., Nix, W., 2004. Sample dimensions influence strength and crystal plasticity. Science 305, 986–989.

Uchic, M., Dimiduk, D., 2005. A methodology to investigate size scale effects in crystalline plasticity using uniaxial compression testing. Mat. Sci. Eng. A 400-401, 268–278.

Uchic, M., Shade, P., Dimiduk, D., 2009. Plasticity of micrometer-scale single crystals in compression: a critical review. Annu. Rev. Mater. Res. 39 (1), 361–386.

Wang, Z.Q., Beyerlein, I.J., LeSar, R., 2009. Plastic anisotropy in fcc single crystals in high rate deformation. Int. J. Plasticity 25 (1), 26–48.

Zhou, C., Biner, S., LeSar, R., 2009. Discrete dislocation dynamics simulations of plasticity at small scales. Acta. Mater. 58 (5), 1565–1577.